Carbon 192 (2022) 133–144

Contents lists available at ScienceDirect

Carbon

journal homepage: www.elsevier.com/locate/carbon

Morphologically tunable nanoarchitectonics of mixed kaolin-halloysite derived nitrogen-doped activated nanoporous carbons for supercapacitor and CO_2 capture applications

Kavitha Ramadass [a, **], CI Sathish [a], Gurwinder Singh [a], Sujanya M. Ruban [a], Ajanya M. Ruban [a], Rohan Bahadur [a], Gopalakrishnan Kothandam [a], Tony Belperio [b], James Marsh [c], Ajay Karakoti [a], Jiabao Yi [a], Ajayan Vinu [a, *]

[a] Global Innovative Center for Advanced Nanomaterials (GICAN), School of Engineering, College of Engineering, Science, and Environment, The University of Newcastle, Callaghan, NSW, 2308, Australia
[b] Minotaur Exploration Pty Limited, 8 Beulah Rd, Norwood, 5067, South Australia, Australia
[c] Andromeda Metals Limited, 69 King William Rd, Unley, 5061, South Australia, Australia

ARTICLE INFO

Article history:
Received 13 December 2021
Received in revised form
14 February 2022
Accepted 21 February 2022
Available online 25 February 2022

Keywords:
Nanoporous
Nanocarbon
Supercapacitance
Heteroatom
Mixed kaolin-halloysite nanoclays
Carbon capture

ABSTRACT

We report an integrated approach by combining in-situ activation, doping and natural nanotemplating to design low-cost and highly efficient N-doped nanoporous carbons for energy storage and carbon capture applications. N-doped nanoporous carbons are prepared by impregnating sucrose, 3-amino 1,2,4-triazole and the $ZnCl_2$ into the nanochannels of the mixed kaolin-halloysite nanotube nanoclay, followed by carbonization and clay template removal. The prepared materials exhibit micro and mesoporosity, high specific surface areas (1360–1695 $m^2\ g^{-1}$), and nitrogen content (7.73–12.34 wt%). The optimized material offers the specific capacitance of 299 F g^{-1} (0.3 A g^{-1}) and 134 F g-1 (10 A g^{-1}) with excellent cycling stability (91% capacity retention after 4000 cycles/5 A g^{-1}). N-doping together with the interconnected micro and mesoporous structure, offers a more ion accessible surface and further provides enhanced charge transfer, hydrophilicity, and the interaction of the electrode-electrolyte ions. The optimized material adsorbs 24.4 mmol g^{-1} of CO_2 at 30 bar pressure and 0 °C. The synthesized materials performed better as supercapacitor and CO_2 adsorbent than halloysite clay, kaolin clay, activated carbon, nanoporous carbons, and mesoporous silica. The method presented here will provide a unique platform for synthesizing a series of advanced nanostructures for electrochemical and carbon capture applications.

1. Introduction

Carbon-based materials have been the recent research focus for energy storage and conversion because these materials can be synthesized from, cheap, non-toxic and sustainable resources [1]. In addition, these carbon-based materials can be easily functionalised with heteroatoms, such as boron (B), nitrogen (N), oxygen (O), sulphur (S), and phosphorus (P) [2,3]. The heteroatom functionalities in carbon-based materials can contribute towards additional pseudo-capacitance, the enhanced electrode surface wettability, and electro-conductivity of the structural framework, thus improving the performance in supercapacitors [3–5]. Many reports are available on the modification of carbon frameworks with heteroatoms such as boron, nitrogen, phosphorus, and sulphur for the applications of energy storage [5–9]. Among these, nitrogen doping has become one of the most critical methods to functionalize carbon since it is more effective in enhancing the wettability, basicity, and its electrical conductivity, which are beneficial for the applications such as CO_2 adsorption, supercapacitors, electrocatalytic reactions, and others [10]. Different strategies have been adopted to synthesize heteroatom doped carbon materials, which include post-synthetic treatment and templating approaches. Post-treatment approach generally involves complex processes and expensive toxic nitrogen precursors such as ammonia or melamine. It has been found that porous carbon materials treated by N-containing precursors such as ammonia, melamine, or others are less favourable for controlling

* Corresponding author.
** Corresponding author.
E-mail address: ajayan.vinu@newcastle.edu.au (A. Vinu).

https://doi.org/10.1016/j.carbon.2022.02.047
0008-6223/

the dopant distribution and the porosity of the materials [11]. In addition, this approach can easily collapse the porous structure.

In contrast to the post-synthetic technique, the templating approach is also a convenient method to develop N-doped porous carbon with ordered porosity by infiltrating single molecular N containing carbon precursors or mixing carbon-nitrogen precursors in the organic/inorganic templates [2]. Wei and his research team [12] adopted templating technique to prepare N-doped ordered mesoporous carbon using resol-dicyandiamide (precursor) and F-127 (template). However, the specific surface area and N content of the material were not high. Another group of researchers [13] also prepared mesoporous N-doped carbon spheres by using dopamine as C-N precursor. Though the N concentration of the synthesized material was relatively high, the BET surface area was only 300–400 $m^2\ g^{-1}$. Mesoporous silica materials were also tried as hard templates to fabricate N-doped ordered mesoporous carbons. For example, Chen et al. [14] fabricated N atom functionalised mesoporous carbons with ordered structure using SBA-15 as a silica template and ionic liquid as C-N source. In another report, Du et al. [15] developed the synthesis approach for N-doped porous carbon using a solid-solid grinding approach in which zeolitic imidazolate framework was impregnated in the porous channels of SBA-15 hard template. Although these methods offered ordered heteroatom functionalised mesoporous carbons, the research in this area was neither advanced nor progressed into commercialization owing to the use of a highly expensive SBA-15 template as its synthesis requires costly precursors and long synthesis time. These challenges may be overcome by replacing these expensive nanotemplates with naturally available and low cost nanotemplates. The naturally occurring kaolin-halloysite nanoclay is a hybrid blend of halloysite and kaolinite clay minerals. Kaolinite has the formula $Al_2Si_2O_5(OH)_4$. $2H_2O$ and typically occurs in platy forms. Halloysite has a similar composition to kaolinite except that it contains additional water molecules between the layers and exhibits a nanotubular morphology. This study provides a convenient and feasible method for utilizing impure HNT (mixed kaolin-halloysite clay), which has poor physical parameters including a low specific surface area, dramatically undermines their overall effectiveness in applications including adsorption and energy storage applications such as supercapacitance and battery.

This study is the first of its kind to report a synthesis strategy for N-doped activated nanoporous carbon (N-ANC) with unique flaky and tubular morphology, tunable high specific surface areas (1360–1695 $m^2\ g^{-1}$), and nitrogen content (7.79–12.34 wt%) through an integrated approach of combined doping, in-situ activation and nanotemplating strategies. The carbon (sucrose) and nitrogen precursor (3-amino-1,2,4-triazole) and the activating source ($ZnCl_2$) were impregnated into the nanochannels of the sacrificial template, the mixed kaolin and halloysite nanotube (K-HNT). We show that N-ANC with high specific surface areas (1360–1695 $m^2\ g^{-1}$), tubular morphology and tunable nitrogen contents can be obtained after the heat treatment followed by the template removal. The optimized material displays a specific capacitance of 299 F g^{-1} at a current density of 0.3 A g^{-1} which surpasses the capacitance of ordered mesoporous carbons prepared from SBA-15, non-activated nanoporous carbons, activated carbons and carbon nanotubes. We also demonstrate that the material with highest specific surface area displayed a high CO_2 adsorption ability (24.4 mmol g^{-1}) at a pressure of 30 bar and a temperature of 0 °C, which exceeds the performance of ordered mesoporous silica, carbon nitrides and ordered mesoporous carbons. This study demonstrates that the mixed kaolin and halloysite nano clay could be a low-cost template for the preparation of series of electrodes and adsorbents for energy storage and carbon capture applications.

2. Materials and methods

2.1. Chemicals and materials

K-HNT which is a mixture of kaolinite and halloysite was sourced from Minotaur Exploration limited, South Australia. The chemicals Sucrose (≥99.5%), 3-amino-1, 2, 4-triazole, zinc chloride, sulphuric acid (98%), and ethanol were sourced from the commercial suppliers.

2.2. Synthesis of N-ANC

N-ANC was fabricated by mixing 3 g of K-HNT nanoclay with a solution containing sucrose (0.9 g), water (4 g), sulphuric acid (0.1 g) and nitrogen precursor, 3-amino-1, 2, 4-triazole (0.35 g). The K-HNT nanoclay and other precursors were thoroughly mixed for about 15–20 min and then heating in a convection air oven at 100 °C for 6 h. Then for another 6 h, heating was continued at 160 °C. It is assumed that the whole solution of carbon and nitrogen precursors entered into the clay template's nanochannels due to the capillary effect and this phenomenon occurred due to the strong attraction between the carbon-containing molecules and the hydroxyl groups of the clay template. After the heat treatment, the sample was pulverized into a fine powder, mixed with $ZnCl_2$ (2 g), and subjected to carbonization at 900 °C for 5 h using a temperature ramp rate of 3 °C/min under nitrogen flow in a horizontal tubular furnace. The powder collected after carbonization was washed with 2 M HCl for 2 h to remove the activating agent. After this, sample was rinsed in distilled water, filtered and dried overnight. Then, the sample was dissolved in diluted HF (5 wt%) solution followed by stirring for about 2 h, filtered and finally washed with ethanol. The filtered sample was dried overnight in a convection oven at 100 °C. A sequence of materials was prepared by carrying the temperature of carbonization within a range of 700–900 °C to tune the nitrogen content and the crystallinity of the samples. The samples are labelled as N-ANCx where x denotes the carbonization temperature. Another batch of samples were fabricated using the N-ANCx synthesis procedure but without the addition of zinc chloride to compare the influence of activation agent on the textural properties and the application performance These samples are named as N-HNCx where x stands for carbonization temperature. To compare the effect of N doping, activated porous carbon nanoflakes were prepared by the procedure reported in our earlier report and the sample was named as AHNC [16].

2.3. Materials characterization

The prepared N-ANCx and A-HNCx materials were characterized with the basic and advanced techniques to understand its structural and textural properties, also their chemical composition and elemental bonding. The surface area of the N-ANCx was determined using a Micromeritics ASAP 2420 instrument at −196 °C. For outgassing before the surface area analysis, all samples were heated at 200 °C under vacuum overnight. BET (Brunauer Emmett-Teller) method was used to calculate Specific surface area (SSA) and the pore volume (Vt) measured at p/p0 = 0.99 was taken as total pore volume. XRD diffraction patterns obtained from Panlytical Empyrean XRD instrument was used to study the structure of N-ANCx. The XRD analysis was carried out by irradiated samples with CuKα1 and Kα2 radiation (λ = 1.5406 Å and 1.5444 Å) at an operating voltage and current of 40 kV and 40 mA, respectively. The XRD patterns were obtained at the wide-angle range of 2θ = 10–80° under continuous scanning with a step size of 0.006°. SEM images obtained with a JEOL scanning electron

microscope (JSM-7900F) was used to investigate the surface morphology of N doped activated carbons The operating voltage for the SEM analysis is 2 kV. The elemental composition of N-ANCx and N-HNCx was estimated using a PerkinElmer instrument (EA 2400) [16]. Raman Spectra was collected from the spectra recorded in the wavenumber range 500–2500 cm^{-1} at a scan rate of 60 cm^{-1} min^{-1}. NEXAFS analysis of the N-ANCx and N-HNCx was done with Soft X-ray spectroscopy beamline attached with a hemispherical electron analyzer in the Australian Synchrotron. The photoelectron current of the photon beam measured on an Au grid was used to normalize the raw NEXAFS data.

2.4. Electrochemical measurement and CO_2 adsorption

Electrochemical measurements were performed on a CHI760 E (CH instruments) work station in 3 M KOH aqueous electrolyte solution using a three-electrode configuration consisting of Ag/AgCl as a reference electrode and platinum rod as a counter electrode. The test electrode was prepared by grinding 4 mg of N-ANCx sample with ethanol (1 ml) and Nafion solution (50 μL of 0.5 wt %). The electrodes were coated on a nickel mesh after the evaporation of the solvent and pressed in a roller.

High-Pressure Volumetric Analyzer (HPVA) equipped with temperature-controlled circulator manufactured by Micromeritics was used to obtain CO_2 adsorption isotherms of a series of synthesized advanced nanostructures at 0–30 bar pressure range. HPVA-200 is the model of the instrument used and the pressure range for this instrument is from vacuum to 200 bars. Three different temperatures of 0, 10, and 25 °C were chosen to analyse the best performing sample to study the effect of temperature on adsorption. The CO_2 adsorption involved initial outgassing of the materials for 10 h at a temperature of 250 °C under a constant vacuum. The adsorption isotherms at three different temperatures were chosen to obtain the isosteric heat of adsorption which was calculated using Clausius-Clapeyron equation.

3. Results and discussion

3.1. Powder XRD analysis

Fig. 1 schematically explains the synthesis method for the preparation of N-ANCx from the naturally available K-HNT template with tunable nitrogen contents and crystallinity. As can be seen in Fig. 1, doping, in-situ activation and nanotemplating processes are combined in a single step to introduce both nanoporosity and N-doping in the porous carbon materials. Sucrose was used as a low-cost carbon precursor whereas 3-amino-1,2,4-triazole was used as a N precursor. The sulphuric acid added in the synthesis acts as a catalyst to dehydrate the carbon precursor, helping in the uniform impregnation of sucrose in the mixed-halloysite template and assisting in the polymerization of sucrose at low temperature [17]. $ZnCl_2$ was used as the activating agent since it is a neutral activating precursor and has a relatively low melting point compared to KOH. It did not generate any caustic reaction when heated with K-HNT template and the carbon-nitrogen precursors. Besides, it helps to synthesize porous carbon nanostructures with both micro and mesoporosity. When K-HNT is heated above 450 °C, dehydroxylation reaction occurs and forms metakaolin an amorphous structure that reacted violently with the gaseous K-salts and generates soluble product with less carbon content which dissolved during the acid washing step [18,19]. Therefore, zinc chloride was chosen as the activation agent. During the high-temperature heating step, the temperature was varied from 700 to 900 °C to tune the N content and the crystallinity of the final porous carbon's nanostructures. After the carbonization and the template removal by acid washing, N-ANCx with high specific surface areas and tunable nitrogen contents are obtained. The crystallinity of the prepared N-ANCx samples was analyzed by powder-XRD diffraction at a wide angle. Fig. 2(a) displays the XRD patterns of the N-ANCx samples. It can be observed that two broad diffraction peaks centered at 2θ of 25 and 43° appeared for all the N-ANCx samples, which correspond to the (002) and (100) plane of the poorly graphitized structure, explaining that the samples are amorphous [20,21]. The absence of the peaks related to the K-HNT reveals that the prepared carbon nanostructures are almost free from the original template materials (Fig. 2(a)). It was found that the peak at 43°, which corresponds to (100) plane, is distinctly visible for N-ANC_{900}, reveals that the graphitic site is intense in this sample, and the interlayer spacing decreases through crystallite growth due to the high-temperature carbonization treatment [22,23]. For comparison, the XRD analysis was also done for N-HNCx samples and the results are presented in Fig. 2(b). These materials showed a slightly increased intensity of the peaks in the region 10–30° which are possibly arising from the presence of K-HNT template. These results suggest that the activation process weakens the aluminosilicate bonding during the treatment with $ZnCl_2$ and supports the easy removal of the template through a simple acid washing process. It should also be noted that the peak at 43° which corresponds to (100) plane of graphitic carbon is absent in these samples, revealing amorphous nature of the sample.

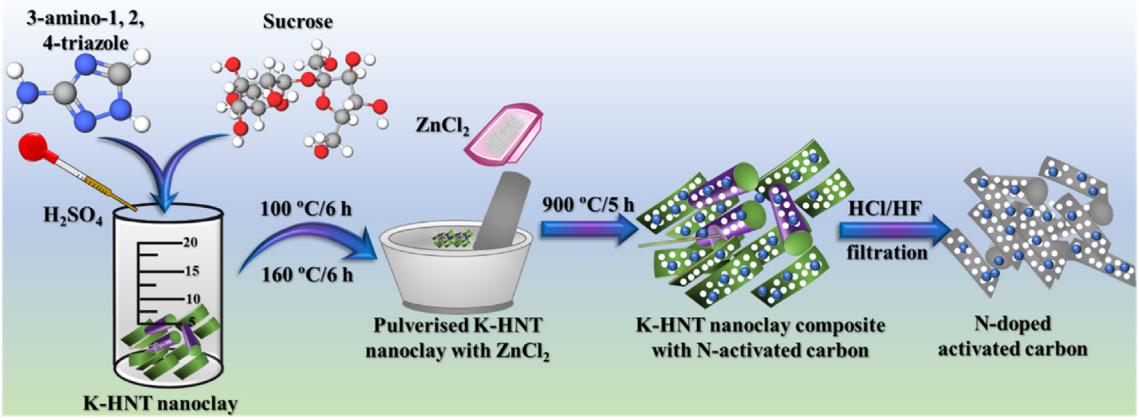

Fig. 1. Schematic representation of the preparation of N-ANCx through integrated doping, insitu activation and nanotemplating approach.

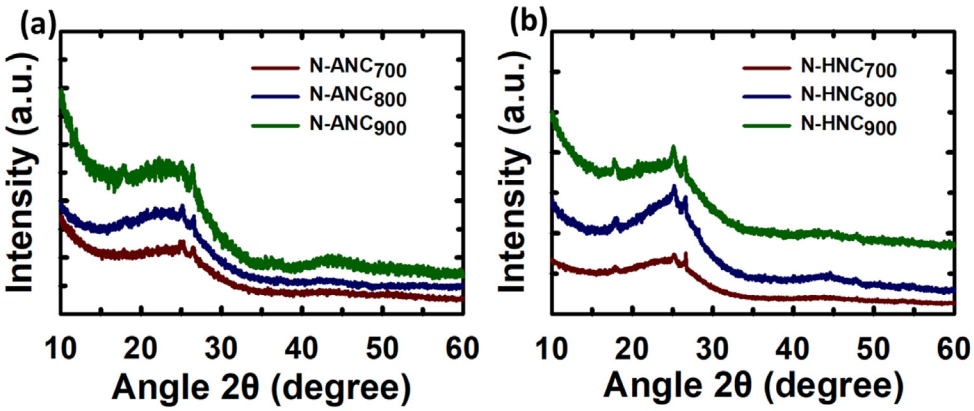

Fig. 2. Wide angle XRD patterns of (a) N-ANCx and (b) N-HNCx.

3.2. Surface area and pore volume analysis

The textural parameters of both activated (N-ANCx) and non-activated (N-HNCx) nanoporous carbon samples were analyzed by nitrogen adsorption measurements. The textural parameters including specific surface area and pore volume are given in Table 1. The isotherm pattern found in N-ANCx and N-HNCx is type IV with hysteresis loops observed at higher relative pressure, which confirms the mesoporosity of the prepared samples [16]. The presence of H3 hysteresis loop at a relative pressure higher than p/p0>0.8 implies that the samples exhibit wide mesopores (Fig. 3) [24]. From the isotherms of the N-HNCx, it can be noticed that less quantity of nitrogen is adsorbed at the low relative pressure and therefore the low-pressure region is almost flat. These data indicate that the samples which are not activated exhibit a small amount of microporosity and therefore the non-activated samples displayed low surface areas. The specific surface areas and the specific pore volumes of N-HNCx lie in the ranges 490–638 $m^2\ g^{-1}$ and 0.77–1.00 $cm^3\ g^{-1}$, respectively. Among the non-activated samples, $N\text{-}HNC_{800}$ displays highest surface area. In contrast, after the activation, the specific surface areas and the pore volumes of the N-ANCx increased quite significantly and lie in the range of 1437–1695 $m^2\ g^{-1}$ and 1.328–1.464 $cm^3\ g^{-1}$, respectively, suggesting that the addition of zinc chloride contributes to the specific surface area and pore volume increment [25,26]. Textural analysis data indicate that the activated material prepared at 800 °C ($N\text{-}ANC_{800}$) exhibits the highest specific surface area (1695 $m^2\ g^{-1}$) and the largest pore volume (1.464 $cm^3\ g^{-1}$) (Fig. S1). It is interesting to note that this material shows high nitrogen adsorption at low-pressure region that is confirmed from the L-shaped isotherm at the low-pressure region, which corresponds to the micropores. Therefore, it can be assumed that the high specific surface area is originated from the micropores generated by the partial decomposition of nitrogen and carbon precursors at a high temperature, assisted by the $ZnCl_2$ activation, and the removal of the K-HNT template and the activating agent [16,26].

3.3. Elemental analysis

Elemental analysis of the N-ANCx and N-HNCx shows that carbonization temperature and the activation process play a predominant role in determining the final composition of the materials, mainly the carbon and the nitrogen content of the prepared samples. Table 1 shows the carbon and nitrogen content for all materials carbonized at different temperatures. The N content in the carbon matrix decreases steadily with an increase in carbonization temperature from 700 to 900 °C owing to the reduced thermodynamic stability of the nitrogen in the structural framework of carbon. Interestingly, the nitrogen content of N-ANCx is in the range of 7.79–11.59 wt% which is higher than that of the N-HNCx, confirming that the activation process suppresses the decomposition of the nitrogen precursor at high carbonization temperature. It is already reported that zinc chloride acts as a stabilizer for N species [27]. In the presence of zinc chloride, the nitrogen precursors can not undergo full decomposition and remain in the carbon framework even at the high carbonization temperatures of ≥700 °C. The gradual melting of Zn leads to good solubility of N atoms owing to the strong Lewis acid-base interactions. Also, the formed ionic melt could catalyse the polymerization of more N atoms to produce an allotrope of graphitic-C_3N_4 [27]. For the activated samples prepared at 700 and 800 °C, at least more than 10 wt % of nitrogen is introduced into the framework of the carbon nanostructures [3,9,21,25]. It is already reported that at 800 °C, the complete reaction occurs between the activating agent and the precursor materials, also the intermediate generated during the carbonization is effectively consumed at this temperature and this indicates activation and carbonization at 800 °C can be considered as an optimum condition to achieve the maximum effect of activation [28]. Raising the carbonization temperature from 800 to 900 °C partially destroys the porosity due to the strong reaction between the activating agent and the template materials and the C and N precursors [19]. Hence, it can be concluded that above 800 °C, the effective utilization of the activating agents would be

Table 1
Textural parameters and elemental composition of N doped porous carbon from mixed kaolin-halloysite nanoclay with and without activation at different carbonization temperatures.

	Sample Code	Carbonization temp °C	Surface Area $m^2\ g^{-1}$	Pore Volume $cm^3 g^{-1}$	C (wt. %)	N (wt. %)	H (wt. %)
Non activated	$N\text{-}HNC_{700}$	700	584	0.855	68.10	10.10	1.63
	$N\text{-}HNC_{800}$	800	638	1.032	68.09	9.53	1.50
	$N\text{-}HNC_{900}$	900	490	1.001	71.91	7.71	1.31
Activated	$N\text{-}ANC_{700}$	700	1571	1.328	64.33	11.59	2.23
	$N\text{-}ANC_{800}$	800	1695	1.464	66.09	10.10	2.54
	$N\text{-}ANC_{900}$	900	1437	1.384	67.61	7.79	1.94

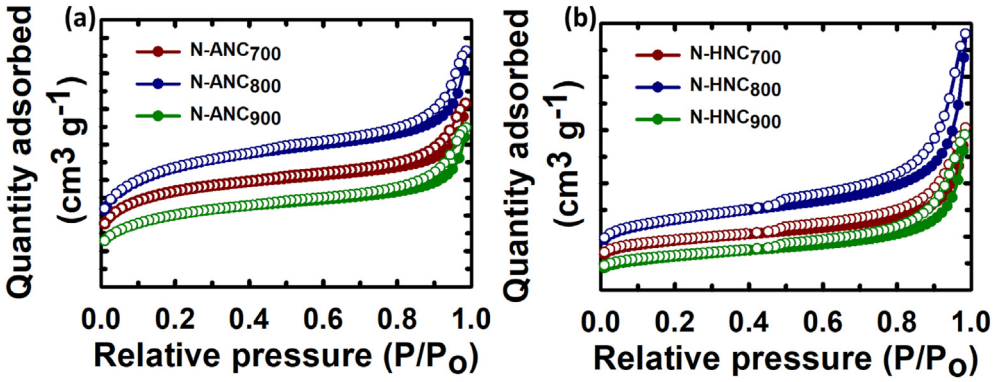

Fig. 3. Nitrogen adsorption-desorption isotherms of (a) N-ANCx, and (b) N-HNCx (Y-axis shifted for clarity and values are not given).

decreased, leading to overactivation, reducing the carbon yield and the specific surface area [29]. From the CHN and nitrogen adsorption analysis, it can be concluded that 800 °C is the optimum temperature to fabricate carbon samples with a well-developed porosity, highest specific surface area and the optimum nitrogen content. It was also observed that N-ANCx were found to be better materials in terms of the nitrogen contents and the textural parameters. Therefore, further characterization was done for only the N-ANCx samples.

3.4. Morphology of N-ANCx

The surface morphology of the materials was investigated using SEM images and the resulting images are shown in Fig. 4. The synthesized N doped activated halloysite nanocarbon materials consist of thin nanosheets of carbon with irregular flaky morphology (Fig. 4(a–c)) and in some places, tubular morphology is observed. It should be noted that the halloysite template used for the replication is a mixed clay material having tubular-shaped halloysite nanotubes and flaky structured kaolinite. Therefore, it is assumed that the observed morphology of the N-ANCx is attributed to the replication of the sheet-like morphology of kaolin in the K-HNT template [16]. Interestingly, the lower magnification TEM image of N-ANC_{800} in Fig. 5 exhibits tubular and flaky carbon, confirming that the tubular structure of the halloysite-kaolinite mixture is also completely replicated into N-ANC_{800}. A clear tubular but disordered pores are also observed from the high-magnified TEM image of N-ANC_{800} (Fig. 5). The halloysite derived nitrogen-doped carbon materials are having disordered micropores and mesopores which improved the textural properties of N-ANCx.

3.5. FT-IR and Raman analysis

Fig. 6(a) presents the FT-IR spectra of N-ANCx materials and the spectra reflect pronounced bands at 3400 and 1730 cm^{-1} which correspond to O-H and C=O stretching vibrations, respectively. These peaks are generated due to the extensive oxidation during the carbonization and the activation process. The other two bands positioned at 2922 and 2853 cm^{-1} identify the C-H vibration of the CH_2 groups in the prepared materials. The peaks positioned around 1424 cm^{-1} and in the region, 1620 to 1640 cm^{-1} indicate C=N and C-N/N-H vibrational stretching that confirms the presence of nitrogen-containing functional groups in the carbon nanostructures [30]. The degree of structural disorder was evaluated by

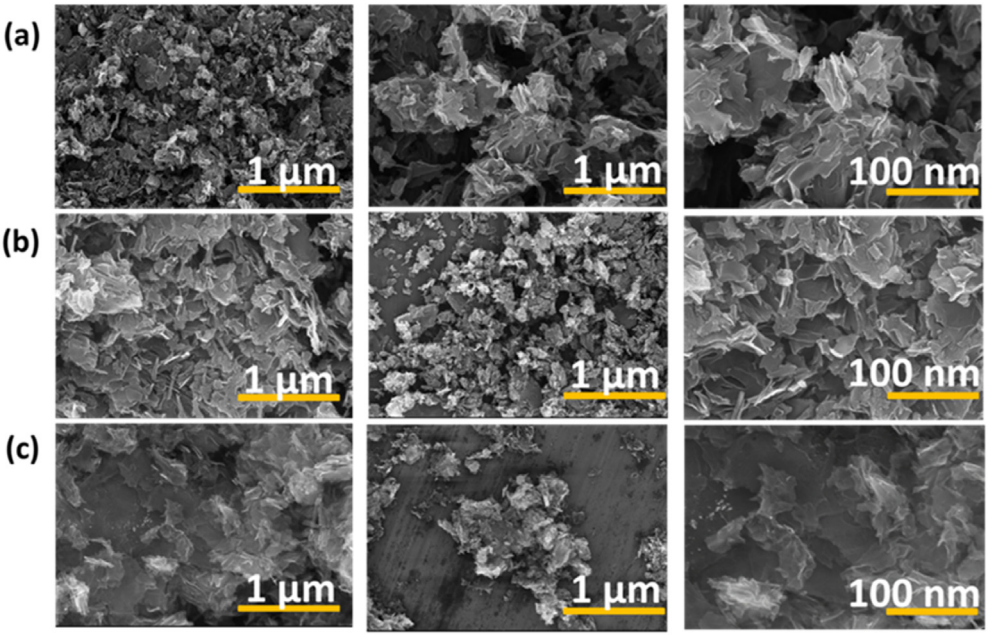

Fig. 4. FE-SEM images of N-ANCx (a) N-ANC_{700} (b) N-ANC_{800} and (c) N-ANC_{900}.

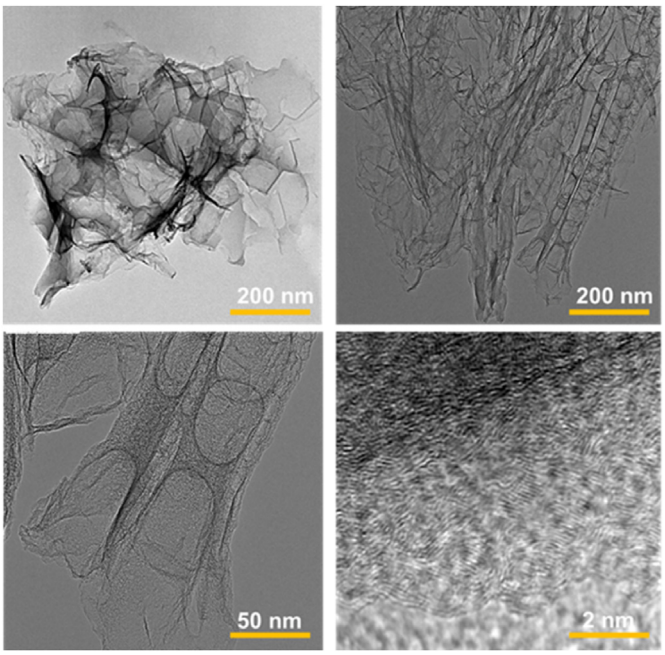

Fig. 5. TEM images of N-ANC$_{800}$ observed at different magnifications.

Raman spectroscopy analysis. In N-ANCx materials, the disorder band (D) band and graphite band (G) are located at 1343 and 1585 cm^{-1} on the Raman spectrum, respectively. The G band is in-plane vibration mode of sp^2 hybridised carbons in the wall structure of N-ANCx whereas the D band is out of plane vibration mode generated due to the defects generated through the nitrogen doping and the dangling bonds at the carbon edges. The ID/IG ratio could be taken as a measure of degree of graphitization. Higher the peak value of D-band indicates the larger the defect degree in the carbon materials and while the higher peak value of G-band means the larger graphitization degree [31]. All of the N-ANCx derived from the K-HNT nanoclay prepared at different temperatures showed an ID/IG ratio higher than 1, indicating that the nitrogen doping created a lot of defects in the carbon nanostructure (Fig. 6(b)). Interestingly, a huge difference in the ID/IG of the samples was observed when the carbonization temperature was changed. The higher ID/IG ratio indicates that the concentration of defects is higher and the samples carbonized at a temperature less than 700 °C showed a higher ratio.

3.6. XPS and NEXAFS analysis

The XPS wide-survey spectra (Fig. 7(a)) clearly showed the peaks of C, N and O at 284.8, 400.0 and 532.8 eV respectively. As demonstrated in Fig. 7(b) and Fig. S2, the deconvoluted C1s spectra of N-ANCx shows five peaks centered around 284.2 (C-C sp2), 285.2 (C-N sp2), 286.4 (C-O), 288.1 (C=O) and 291.8 eV (CO*) OH groups [27–30]. Deconvoluted N1s spectra (Fig. 7(c)) shows four peaks centered at 397.8, 399.28 400.44 and 403.09 eV, represents pyridinic-N (397.8 eV), pyrrolic-N (399.28 eV), graphitic-N (400.44 eV) and oxidized-N (403.09 eV) respectively [28]. The predominant nitrogen groups in all the N-ANCx samples are pyridinic-N along with and pyrrolic-N. Pyridine-N-oxide and the quaternary nitrogen are the nitrogen functional groups present in the samples treated with high temperature which are found in N-ANCx samples, because of the high activation temperature in this study. These results illustrate that nitrogen functional groups are indeed incorporated into the activated nanoporous carbon samples. The deconvoluted O1s spectra given in Fig. 7(d) display three peaks which are centered around 530.5, 532.1, and 535.2 that can be assigned to C=O, (CO*) OH, and C-O-C, respectively [32]. These peaks strongly indicate that a combination of activation and carbonization at high-temperature support extensive oxidation which creates oxygen group functionalities on the carbon surface. The oxygen and nitrogen-containing functional groups could be beneficial in the adsorption of carbon dioxide molecules and can also effectively contribute to the surface redox reactions that support energy storage applications [33].

Near edge X-ray Absorption Fine Spectroscopy (NEXAFS) is a versatile analytical technique to study the elemental binding of materials. Fig. 8(a) displays the normalized spectra of the C K-edge spectra of N-ANC$_{800}$ and N-HNC$_{800}$. These samples show three peaks which are assigned to C1 at ~285.43 eV, corresponding to C=C bond, C2 at ~288.3 eV, corresponding to C-N bond and C3 at ~291.2 eV, assigned to σ* associated with either C-C or C-N. NEXAFS spectra also show three different chemical states of N in the samples. The N K-edge spectra of the N-ANCx show three pronounced p*-resonances at 397.9, 399.5 and 401.1 eV (Fig. 8(b)). The peak 1 at 398.3 eV and peak 3 at 401.1 eV are generally attributed to pyridinic and pyrrolic nitrogen, respectively whereas the peak 2 is very different, and is attributed to the nitrogen in the amino groups attached with the carbon matrix, corresponding to C=N [34]. The NEXAFS result is another supporting evidence to confirm that the N is incorporated into the carbon matrix of the N-ANCx.

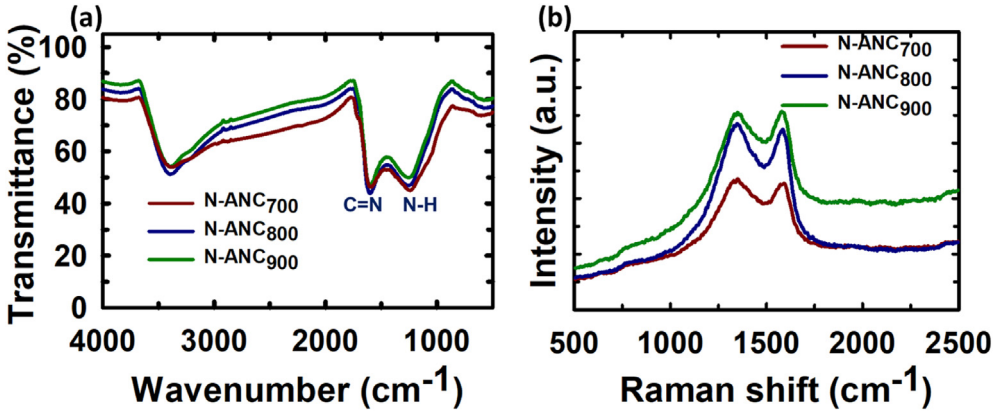

Fig. 6. (a) FT-IR spectra, and (b) Raman spectra of N-ANCx.

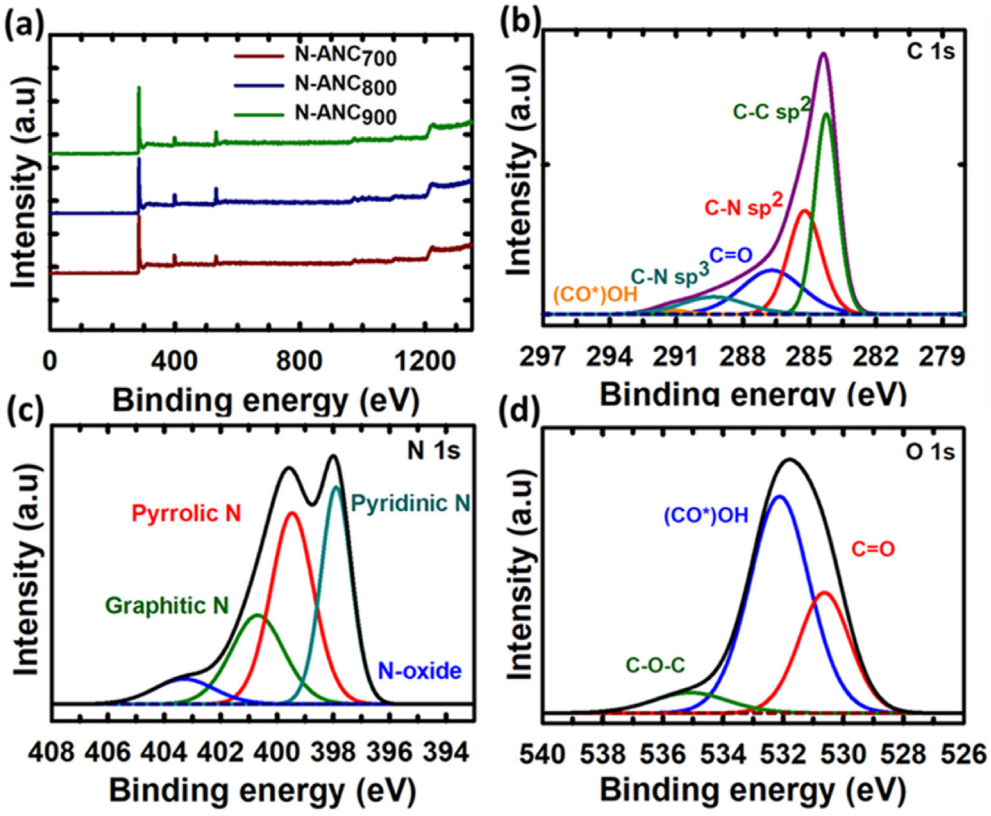

Fig. 7. (a) XPS survey spectra of N-ANCx, and high-resolution spectra of N-ANC$_{800}$ (b) C1s (c) N1s and (d) O 1s. (A colour version of this figure can be viewed online.)

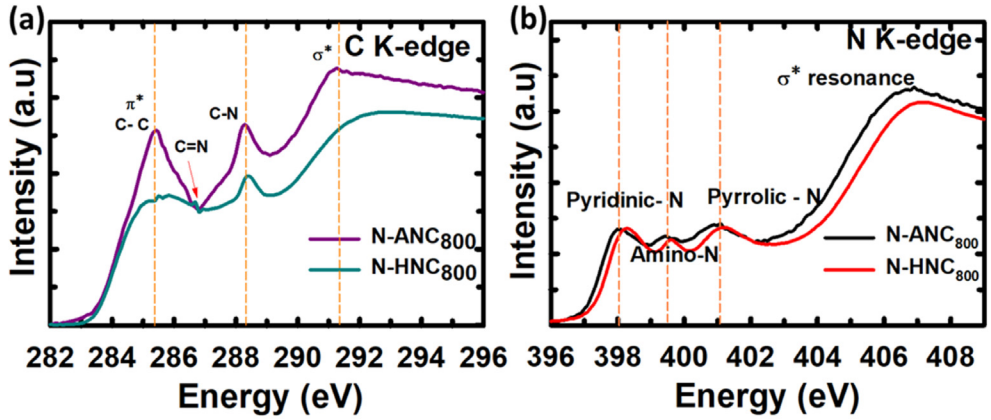

Fig. 8. NEXAFS data of N-ANC$_{800}$ and N-HNC$_{800}$ (a) C_K edge (b) N_K edge.

3.7. Performance of N-ANC materials as supercapacitors

The N-ANCx samples were used to fabricate electrodes and tested for supercapacitor performance in a standard method of electrode testing using a three-electrode cell configuration. The electrolyte used for the capacitance measurement is 3 M aqueous KOH. The scan rate for obtaining the cyclic voltammetry (CV) curves was varied from 5 to 100 mV s^{-1}. The CV curves show a nearly rectangular shape which indicates the superior charge storage ability and high efficiency, and this also confirms that N-ANCx materials possess the characteristics of an ideal electrical double-layer capacitor (EDLC). It should be noted that the shape of the CV curve in N-ANC$_{700}$ sample is not as rectangular as N-ANC$_{800}$ and N-ANC$_{900}$. The quasi-rectangular shape of the CV curves of N-ANC$_{800}$ and N-ANC$_{900}$ is retained even when the scan rate ramped up to 100 mV s^{-1} which implied a rapid electron transport in the charge/discharge cycling process. The current density range selected for the galvanostatic charge-discharge (GCD) cycling process is from 0.3 to 10 A g^{-1} and the GCD profiles of the N-ANCx materials revealed no significant drop in the IR voltage and the shape of the profiles is almost linear and symmetrical, which confirms that N-ANC$_{800}$ and N-ANC$_{900}$ materials have high specific capacitance and can be an efficient electrode for the electrical double layer capacitor (Fig. 9(a–f)).

Fig. 10(a) displays the CV curves of the N-ANCx materials obtained at the scan rate of 10 mV s^{-1} and this clearly explained that the quasi-rectangular shape of N-ANC$_{800}$ and N-ANC$_{900}$ is better than the CV of N-ANC$_{700}$ sample. The specific capacitance of N-

ANC_{900} at a current density of 0.3 A g^{-1} is 299 F g^{-1} which drops to 194 F g^{-1} when the current density is increased to 1 A g^{-1}. Among the N-ANCx materials studied, N-ANC_{900} registers the highest capacitance (194 F g^{-1}) than N-ANC_{800} (183 F g^{-1}) and N-ANC_{700} (151 F g^{-1}) at 1A g^{-1} even though N-ANC_{800} exhibits the highest specific surface area and the pore volume (Fig. 10(b)). The material N-ANC_{900} exhibited a higher capacitance value (194 F g^{-1}/1A g^{-1}) than our previously reported material AHNC which is the activated porous carbon nanoflakes derived from halloysite nanotubes without N-doping (158 F g^{-1}/1A g^{-1}) [16]. Generally, at higher current densities, a lower capacitance value is observed due to the shorter time for the electrolyte ions permeation into the electrode materials [2,35,36]. However, N-ANC_{800} and N-ANC_{900} materials provide an abundant inner surface for good diffusion of electrolyte ions even at higher current densities, hence fairly high specific capacitance of 148 F g^{-1} at 10 A g^{-1} current density was noticed, demonstrating their better capacitance ability at higher current densities. Electrochemical Impedance (EIS) analysis was also conducted to investigate the electrochemical behaviour of the electrodes prepared using N-ANCx samples and Nyquist plots were obtained from the EIS analysis (Fig. 10(c)). A typical Nyquist plot of EDLC shows a semi-circular curve in the high-frequency and a vertical straight line at the low-frequency zones. The Nyquist plots of N-ANC_{800} and N-ANC_{900} show a perpendicular line in the low-frequency area which confirms the good electrochemical behaviour and also quick permeation of electrolyte ions in the material's surface. The semi-circular arc noticed in the high-frequency Nyquist plot of N-ANC_{800} and N-ANC_{900} samples implies a fast electron transport between the electrodes and the electrolyte. It is found that the supercapacitance value obtained for N-ANC_{900} (Fig. 10(d) & Table 2) in this work exceeds the supercapacitance value reported for the commercially available single and multi-walled walled CNTs, activated carbon, ordered mesoporous carbons, activated porous carbon from HNT and few other carbon-based materials reported so far [41]. Table S3 highlights that N-ANC_{900} outweighs the performance of N-doped porous carbon

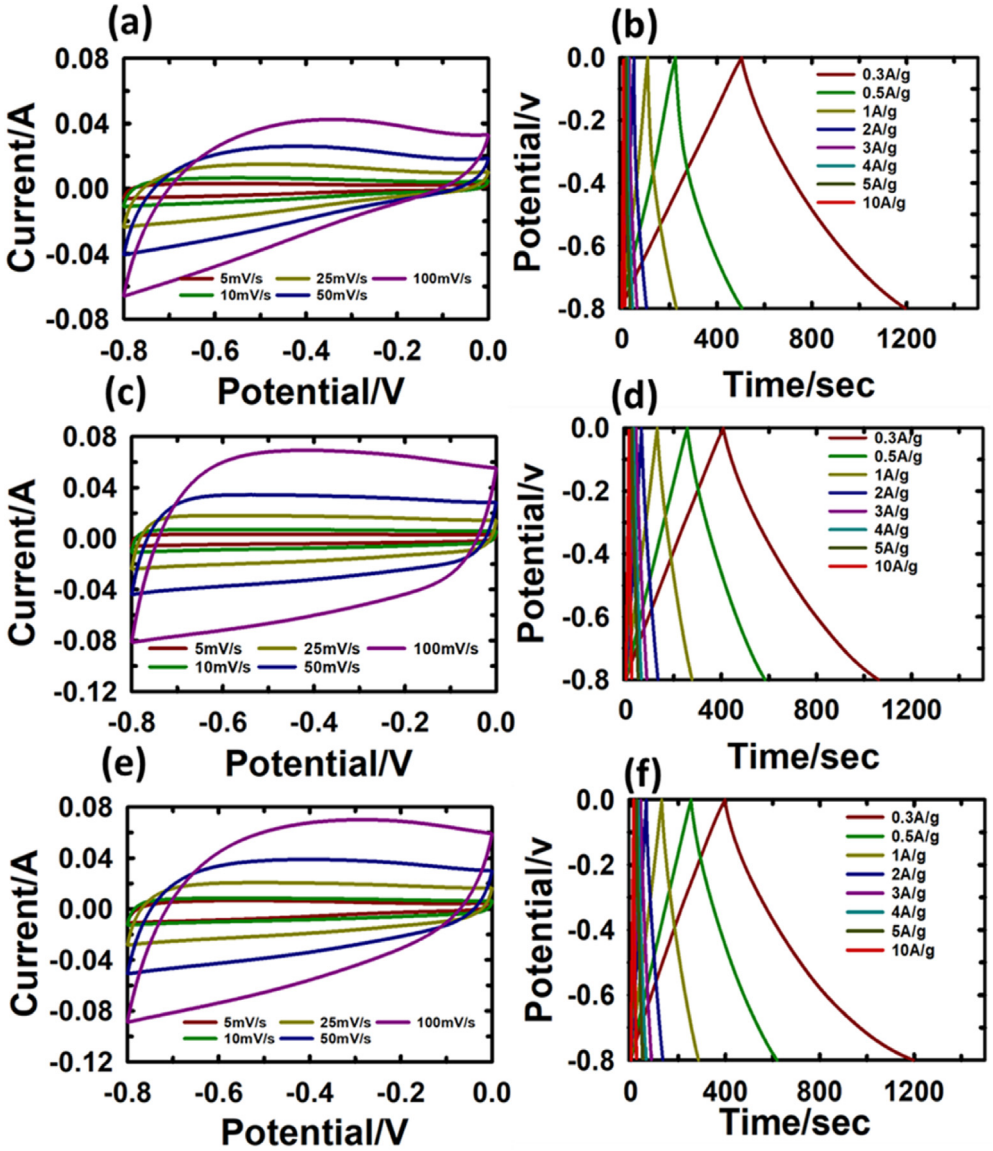

Fig. 9. Cyclic voltammograms (CV) of the samples measured between the scan rate range of 5–100 mV s^{-1} (a) N-ANC_{700} (c) N-ANC_{800} and (e) N-ANC_{900}; Galvanostatic charge/discharge (GCD) measurements of N-ANCx samples measured at different current densities in the range of 0.3–10 A g^{-1} (b) N-ANC_{700} (d) N-ANC_{800} and (f) N-ANC_{900}. (A colour version of this figure can be viewed online.)

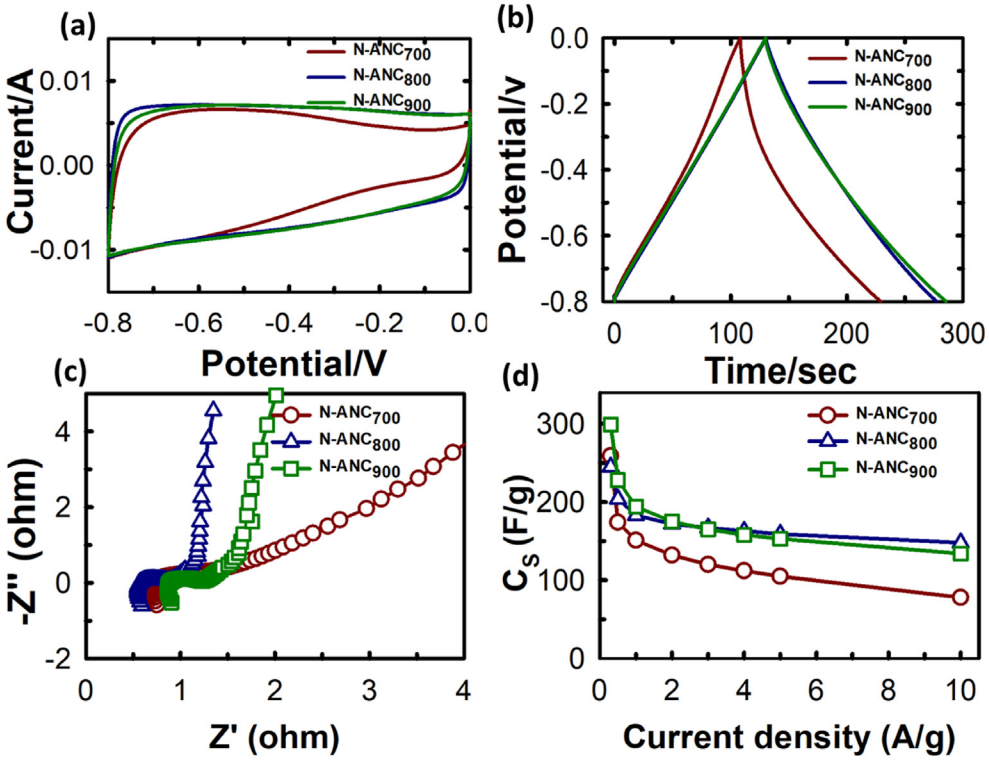

Fig. 10. Specific capacitance data of N-ANC$_X$ (a) Cyclic voltammograms (CV) of the samples measured at scan rate-10 mV s^{-1} (b) Galvanostatic charge/discharge (GCD) measurements of N-ANCx samples measured at the current density of 1 A g^{-1} (c) The Nyquist plot of N-ANCx samples measured at 0.1 hz and (d) Specific capacitance value (Cs) of N-ANCx samples measured at various current densities.

materials such as nitrogen-doped carbon nanofibres, casein-derived porous carbon, coffee waste-derived nitrogen-doped carbon reported in the recent literature. The exceptional performance of N-ANC$_{900}$ is because of the homogeneous N doping into the nanostructure of porous carbon, which enhances surface wettability. A combination of high specific surface area and large pore volume originating from the interconnected meso and micro-channels in the tubular network further improves the rate performance. The enhanced electrochemical behaviour of N-ANC$_{900}$ is due to the perfect nanoarchitecture, which is favourable for more ions access and fast diffusion. The presence of hierarchical pore distribution offers an advantage in enhancing electrochemical behavior. The microporous structure helps to create the electrical double layers, and the mesopores shorten the length between the electrolyte-electrode interface [35–41]. The cycling performance test was done for N-ANC$_{900}$ material. The specific capacitance retention is about 91% even after long runs of the charge/discharge process (4000 Cycles at 5 A g^{-1} current density), suggesting that the electrodes prepared from N-ANC$_{900}$ material are highly stable and have excellent cycling performance (Fig. S3). It is known that the carbon framework collapses when the heteroatoms is loaded in high amounts, which leads to the reduced stability of the electrodes; however, in this study, high N doping was successfully done through an effective combined in-situ nanotemplating and activation approach. The excellent cycling ability of the electrode fabricated from N-ANC$_{900}$ suggests that N atoms are successfully incorporated in the nanoporous carbon framework without affecting its nanostructure [40]. Although N-ANC$_{800}$ possesses the highest specific surface area, the specific capacitance is lower than N-ANC$_{900}$. This could be due to a combination of a high specific surface area, high nitrogen content and most importantly, high crystallinity generated at a high carbonization temperature that contributed towards superior specific capacitance for the material prepared at 900 °C. The excellent performance of N-ANC$_{900}$ reveals the importance of the combined treatment of doping, templating and activation adopted in this work. The excellent textural parameters, when combined with the crystallinity, uniform distribution of N atoms in the porous carbon structure and oxygen functional groups generated through the extensive oxidation, occurred due to the high-temperature carbonization and activation with $ZnCl_2$, helps to achieve the superior specific capacitance for the N-ANC$_{900}$.

Table 2
Supercapacitance values of N doped activated nanoporous carbon prepared at different carbonization temperature.

Current Density (A g^{-1})	N-ANC$_{700}$ (F g^{-1})	N-ANC$_{800}$ (F g^{-1})	N-ANC$_{900}$ (F g^{-1})
0.3	259	245	299
0.5	174	204	228
1	151	183	194
2	132	172	175
3	120	167	165
4	112	163	158
5	105	159	153
10	78	148	134

3.8. Performance of N-ANC materials as CO_2 adsorbents

As the N-ANCx materials exhibit unique tubular morphology with interconnected micro and mesopores and high specific surface area, we employed them as adsorbents for the CO_2 uptake. The CO_2 adsorption measurements were performed with N-ANCx samples at 0 °C and the isotherms are given in Fig. 11(a). Fig. 11 (a) displays the amount of CO_2 adsorption in the samples that increase linearly

to the increase in the adsorption pressure and reaches a maximum at 30 bar [42]. At low pressure, the CO_2 molecules generally occupy the micropores whereas the mesopores in the tubular structures are filled at high pressure as it supports the dense packing of the molecules and further forces the molecules to reach the adsorption sites located deep insides the pores. The CO_2 adsorption capacity of N-ANC_{800} is 24.4 mmol g^{-1} at 0 °C and 30 bar, which is better when compared to N-ANC_{700} (21.6 mmol g^{-1}) and N-ANC_{900} (17.9 mmol g^{-1}). A high CO_2 uptake of N-ANC_{800} is attributed to its superior textural properties such as the higher specific surface area and larger pore volume when compared to N-ANC_{900} and N-ANC_{700} samples. It is also believed that the electronic interaction between the nitrogen functional groups on the surface of the adsorbent and the incoming CO_2 molecules enhances the capability of the N-ANC_{800} to adsorb more CO_2 molecules. The CO_2 adsorbed at low pressure is much higher for N-ANC_{800} and N-ANC_{700} than that of N-ANC_{900}. A large amount of nitrogen on the surface of the N-ANC_{800} and N-ANC_{700} is responsible for the large adsorption at low pressure. When the adsorption capacity of these materials at high pressure is compared, N-ANC_{800} registers the highest adsorption capacity even though N-ANC_{700} has the highest amount of nitrogen. This is attributed to the loss of the adsorption sites due to the lower specific surface area which leads to a reduction in the amount of CO_2 adsorption. These data reveal that the optimum amount of nitrogen together with the enhanced textural properties are important to achieve higher CO_2 adsorption capacity.

The temperature effect on the CO_2 adsorption capacity of N-ANC_{800} was investigated by performing the CO_2 adsorption measurements at various temperatures including 0 °C, 10 °C, and 25 °C with pressure varying from 0 to 30 bar (Fig. 11 (b)). At a low pressure of 1 bar, the material adsorbed 3.9 mmol g^{-1} of CO_2 which increased to 24.2 mmol g^{-1} at 30 bar (Fig. 11(a)). The effect of the temperature on the CO_2 adsorption capacity of N-ANC_{800} shows that it decreases with an increase in the adsorption temperature. For example, at the low pressure of 1 bar, the CO_2 adsorption capacity at 25 °C is 2.0 mmol g^{-1}, which is almost half of what is observed at 0 °C. These results suggest that the adsorption of CO_2 molecules in N-ANC_{800} is more favourable at lower temperatures which indicates that the adsorption is exothermic. The adsorption isotherms collected at three different temperatures were used to calculate the isosteric heat of adsorption with the formula derived by Clausius and Clapeyron (Fig. 11(c)). The isoelectric heat of adsorption falls in the range 31.9 to 24.8 kJ mol^{-1}, which is lower than the values reported for the chemisorption [43,44]. The lower value of isosteric heat of adsorption suggests that the interactions between the adsorbent and mildly acidic CO_2 molecules are moderate, and the mode of adsorption is physical in nature [45]. It is generally believed that, for porous materials such as carbon, the main determining factor for the adsorption of CO_2 molecules is the specific surface area. However, the presence of nitrogen functional groups on the surface also plays an important role in boosting the CO_2 and adsorbent interactions. This is confirmed by the results that the porous carbon derived from HNT without any nitrogen doping adsorbed only 13.7 mmol g^{-1} which is much lesser as compared to the adsorption ability of the N-ANC_{800} (24.4 mmol g^{-1}) (Fig. 11(d)). These results point out that both the pore structure and N-doping in N-ANC_{800} significantly influence the high-pressure CO_2 adsorption capacity. The introduction of nitrogen not only improves the electron density of the carbon structure but also introduces Lewis basic sites which will enhance the adsorption of the CO_2 molecules through Lewis-acid (CO_2)/ Lewis-base (N atoms in the carbon nanostructure of N-ANC_{800})

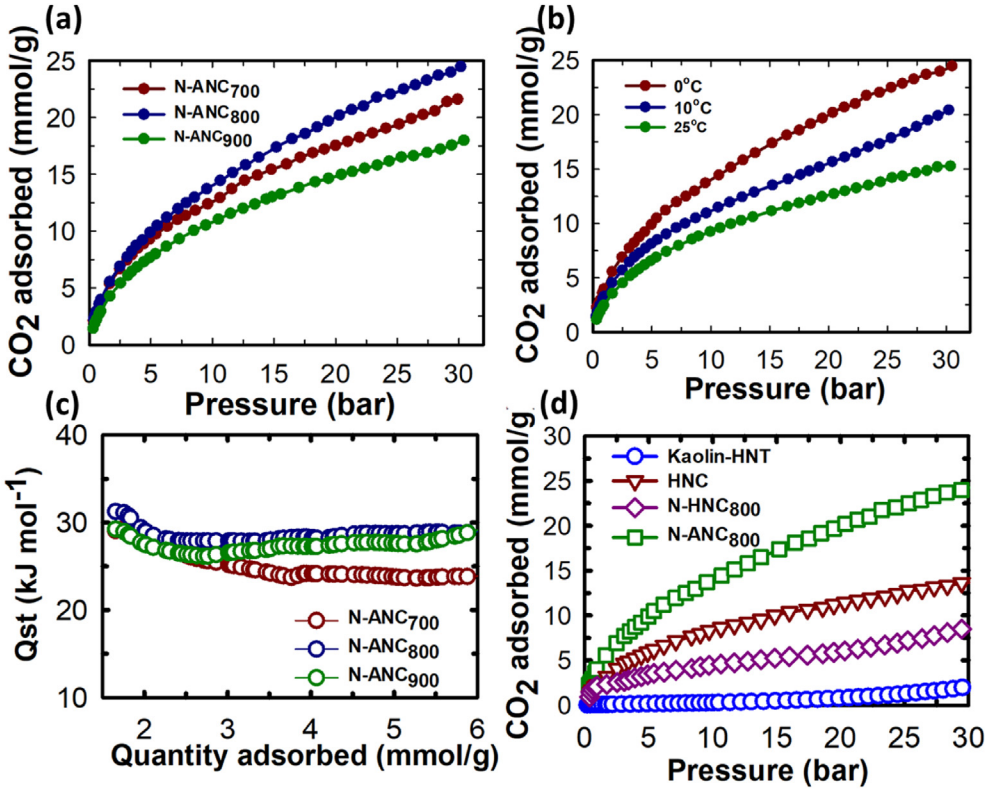

Fig. 11. The CO_2 adsorption isotherms of a) N-ANCx samples measured at a pressure range of 0–30 bar, and b) N-ANC_{800} measured at three different temperatures 0, 10 and 25 °C and a common pressure range of 0–30 bar c) Isosteric heat of adsorption of N-ANCx samples calculated from adsorption isotherms obtained at three different temperatures of 0, 10 and 25 °C and d) Comparison of N-ANC_{800} with the K-HNT and other porous carbon materials: HNC- Porous carbon derived from K-HNT; N-HNC_{800} – N doped porous carbon derived from K-HNT without activation. (A colour version of this figure can be viewed online.)

interactions [2]. In Table S4, the adsorption performances of N-ANCx are also compared with other relevant porous carbon materials. The comparison of the CO_2 adsorption of N-ANCx was done with the nitrogen functionalised mesoporous carbons, N-doped activated carbon and mesoporous carbon nitrides and the data revealed that N-ANCx has high CO_2 adsorption capacity than the compared materials owing to its superior textural properties and nitrogen doping. In addition, the CO_2 adsorption capacity of N-ANC_{800} is far better than other materials such as CNTs (both single-walled and multi-walled), activated carbons, mesoporous carbons, mesoporous silica, and mesoporous carbon nitrides [16]. However, few other studies reported nitrogen functionalised porous carbon-based adsorbents with high CO_2 adsorption, but these materials require a complex synthesis process and expensive chemicals. The high CO_2 adsorption capacities of the synthesized materials N-ANCx from a low-cost and straightforward strategy present a huge potential in this field. Moreover, the abundant availability of natural halloysite and the low cost of other starting precursors are attractive prospects for commercialization.

This paper discloses a straightforward synthesis strategy to fabricate N-doped activated carbon nanostructures in which carbon precursor, nitrogen precursor and the activating agent ($ZnCl_2$) were all impregnated in a mixed kaolin-halloysite template in a single step. The synthesis method has the advantages that the non-toxic precursor is taken as a carbon source, and novel nitrogen precursor is used as the nitrogen source, and the characteristics of low production cost and simple preparation process are achieved. The nitrogen-doped activated carbons with different nitrogen contents and specific surface areas can be prepared by controlling the ratio of the carbon source to the nitrogen source and selecting an appropriate carbonization temperature. The synthesized nitrogen-doped activated carbon can serve as an electrode material, and an adsorbent.

4. Conclusions

This work presented an efficient and straightforward approach for synthesizing N-doped activated nanoporous carbon with flake and tubular morphology from inexpensive and naturally abundant halloysite template. The approach involved an integration of in-situ doping, activation and nanotemplating with natural nanoclays. The synthesized materials exhibited large specific surface areas, pore volumes and tunable nitrogen content. The optimized nitrogen-doped nanoporous carbon material with the high crystallinity outperformed other nanoporous carbon materials, activated carbon and carbon nanotubes by showing a specific capacitance of 299 F g^{-1} at a current density of 0.3 A g^{-1}, while the sample with the optimized surface area and nitrogen content prepared at 800 °C exhibited a high CO_2 uptake ability of 24.4 mmol g^{-1} at 0 °C and 30 bar. The templating and activation induced both micropores and mesopores which may be responsible for the high specific surface area, more active sites, and more surface functional groups, leading to high-performance supercapacitor and CO_2 adsorption ability. We strongly believe that the innovative approach demonstrated in this work will provide a novel platform for the design of a series of low cost and advanced nanoporous materials with exciting textural properties and heteroatoms which may be of benefit for various fields such as gas adsorption, separation, catalysis and the energy-related storage applications.

CRediT authorship contribution statement

Kavitha Ramadass: Conceptualization, Writing – original draft, Investigation, Methodology, Visualization. **CI Sathish:** Investigation. **Gurwinder Singh:** Writing – review & editing. **Sujanya M. Ruban:** Investigation. **Ajanya M. Ruban:** Investigation. **Rohan Bahadur:** Investigation. **Gopalakrishnan Kothandam:** Investigation. **Tony Belperio:** Supervision, Funding acquisition. **James Marsh:** Supervision, Funding acquisition. **Ajay Karakoti:** Writing – review & editing. **Jiabao Yi:** Writing – review & editing. **Ajayan Vinu:** Conceptualization, Funding acquisition, Supervision, Writing – review & editing.

Declaration of competing interest

The authors declare that they have no known competing financial interests or personal relationships that could have appeared to influence the work reported in this paper.

Acknowledgments

The authors acknowledge financial support from Minotaur Exploration Pty Limited and the Department of Industry, Innovation and Science through an Innovation Connection Grant.

Appendix A. Supplementary data

Supplementary data to this article can be found online at https://doi.org/10.1016/j.carbon.2022.02.047.

References

[1] D. Yu, Y. Ma, M. Chen, X. Dong, KOH activation of wax gourd-derived carbon materials with high porosity and heteroatom content for aqueous or all-solid-state supercapacitors, J. Colloid Interface Sci. 537 (2019) 569–578.
[2] S. Wang, J. Qin, Y. Zhao, L. Duan, J. Wang, W. Gao, R. Wang, C. Wang, M. Pal, Z.-S. Wu, W. Li, D. Zhao, Ultrahigh surface area N-doped hierarchically porous carbon for enhanced CO_2 capture and electrochemical energy storage, ChemSusChem 12 (15) (2019) 3541–3549.
[3] Y. Zhou, A.M. LaChance, A.T. Smith, H. Cheng, Q. Liu, L. Sun, Strategic design of clay-based multifunctional materials: from natural minerals to nano-structured membranes, Adv. Funct. Mater. 29 (16) (2019), 1807611.
[4] G. Zhao, C. Chen, D. Yu, L. Sun, C. Yang, H. Zhang, Y. Sun, F. Besenbacher, M. Yu, One-step production of O-N-S co-doped three-dimensional hierarchical porous carbons for high-performance supercapacitors, Nano Energy 47 (2018) 547–555.
[5] Y. Zhang, C. Sun, Z. Tang, High specific capacitance and high energy density supercapacitor electrodes enabled by porous carbon with multilevel pores and self-doped heteroatoms derived from Chinese date, Diam. Relat. Mater. 97 (2019), 107455.
[6] X. Kang, H. Zhu, C. Wang, K. Sun, J. Yin, Biomass derived hierarchically porous and heteroatom-doped carbons for supercapacitors, J. Colloid Interface Sci. 509 (2018) 369–383.
[7] J.-S.M. Lee, M.E. Briggs, C.-C. Hu, A.I. Cooper, Controlling electric double-layer capacitance and pseudocapacitance in heteroatom-doped carbons derived from hypercrosslinked microporous polymers, Nano Energy 46 (2018) 277–289.
[8] J.-G. Wang, H. Liu, H. Sun, W. Hua, H. Wang, X. Liu, B. Wei, One-pot synthesis of nitrogen-doped ordered mesoporous carbon spheres for high-rate and long-cycle life supercapacitors, Carbon 127 (2018) 85–92.
[9] K. Zou, Y. Deng, J. Chen, Y. Qian, Y. Yang, Y. Li, G. Chen, Hierarchically porous nitrogen-doped carbon derived from the activation of agriculture waste by potassium hydroxide and urea for high-performance supercapacitors, J. Power Sources 378 (2018) 579–588.
[10] T. Liu, L. Zhang, W. You, J. Yu, Core–shell nitrogen-doped carbon hollow spheres/Co_3O_4 nanosheets as advanced electrode for high-performance supercapacitor, Small 14 (12) (2018), 1702407.
[11] Y. Deng, Y. Xie, K. Zou, X. Ji, Review on recent advances in nitrogen-doped carbons: preparations and applications in supercapacitors, J. Mater. Chem. 4 (4) (2016) 1144–1173.
[12] J. Wei, D. Zhou, Z. Sun, Y. Deng, Y. Xia, D. Zhao, A controllable synthesis of rich nitrogen-doped ordered mesoporous carbon for CO_2 capture and supercapacitors, Adv. Funct. Mater. 23 (18) (2013) 2322–2328.
[13] J. Tang, J. Liu, C. Li, Y. Li, M.O. Tade, S. Dai, Y. Yamauchi, Synthesis of nitrogen-doped mesoporous carbon spheres with extra-large pores through assembly of diblock copolymer micelles, Angew. Chem. Int. Ed. 54 (2) (2015) 588–593.
[14] A. Chen, Y. Yu, R. Wang, Y. Yu, W. Zang, P. Tang, D. Ma, Nitrogen-doped dual mesoporous carbon for the selective oxidation of ethylbenzene, Nanoscale 7 (35) (2015) 14684–14690.
[15] J. Du, R. Liu, Y. Yu, Y. Zhang, Y. Zhang, A. Chen, N-doped ordered mesoporous carbon prepared by solid–solid grinding for supercapacitors, J. Mater. Res. 33

(20) (2018) 3408–3417.
[16] K. Ramadass, C.I. Sathish, S. MariaRuban, G. Kothandam, S. Joseph, G. Singh, S. Kim, W. Cha, A. Karakoti, T. Belperio, J.B. Yi, A. Vinu, Carbon nanoflakes and nanotubes from halloysite nanoclays and their superior performance in CO_2 capture and energy storage, ACS Appl. Mater. Interfaces 12 (10) (2020) 11922–11933.
[17] R. Ryoo, S.H. Joo, S. Jun, Synthesis of highly ordered carbon molecular Sieves via template-mediated structural transformation, J. Phys. Chem. B 103 (37) (1999) 7743–7746.
[18] Y. Gao, Q. Yue, B. Gao, A. Li, Insight into activated carbon from different kinds of chemical activating agents: a review, Sci. Total Environ. 746 (2020), 141094.
[19] M. Mahloujifar, M. Mansournia, Kaolinite fusion in carbonate media: $KAlSiO_4$–$NaAlSiO_4$ phase transformations and morphological study, Mater. Res. Express 6 (2) (2018), 025040.
[20] Y. Lu, L. Wang, K. Preuß, M. Qiao, M.-M. Titirici, J. Varcoe, Q. Cai, Halloysite-derived nitrogen doped carbon electrocatalysts for anion exchange membrane fuel cells, J. Power Sources 372 (2017) 82–90.
[21] G. Singh, K. Ramadass, J.M. Lee, I.S. Ismail, M. Singh, V. Bansal, J.-H. Yang, A. Vinu, Convenient design of porous and heteroatom self-doped carbons for CO_2 capture, Microporous Mesoporous Mater. 287 (2019) 1–8.
[22] K. Shi, J. Yang, J. Li, X. Zhang, W. Wu, H. Liu, S.-H. Yoon, X. Li, Effect of oxygen-introduced pitch precursor on the properties and structure evolution of isotropic pitch-based fibers during carbonization and graphitization, Fuel Process. Technol. 199 (2020), 106291.
[23] G. Singh, K.S. Lakhi, K. Ramadass, C.I. Sathish, A. Vinu, High-performance biomass-derived activated porous biocarbons for combined pre- and post-combustion CO_2 capture, ACS Sustain. Chem. Eng. 7 (7) (2019) 7412–7420.
[24] M.R. Benzigar, S. Joseph, G. Saianand, A.-I. Gopalan, S. Sarkar, S. Srinivasan, D.-H. Park, S. Kim, S.N. Talapaneni, K. Ramadass, A. Vinu, Highly ordered iron oxide-mesoporous fullerene nanocomposites for oxygen reduction reaction and supercapacitor applications, Microporous Mesoporous Mater. 285 (2019) 21–31.
[25] S. Li, Q. Gu, N. Cao, Q. Jiang, C. Xu, C. Jiang, C. Chen, C. Pham-Huu, Y. Liu, Defect enriched N-doped carbon nanoflakes as robust carbocatalysts for H_2S selective oxidation, J. Mater. Chem. 8 (18) (2020) 8892–8902.
[26] G. Singh, K.S. Lakhi, I.Y. Kim, S. Kim, P. Srivastava, R. Naidu, A. Vinu, Highly efficient method for the synthesis of activated mesoporous biocarbons with extremely high surface area for high-pressure CO(2) adsorption, ACS Appl. Mater. Interfaces 9 (35) (2017) 29782–29793.
[27] B. Liu, R. Shi, R. Chen, C. Wang, K. Zhou, Y. Ren, Z. Zeng, Y. Liu, L. Li, Optimized synthesis of nitrogen-doped carbon with extremely high surface area for adsorption and supercapacitor, Appl. Surf. Sci. 538 (2021), 147961.
[28] G. Singh, I.Y. Kim, K.S. Lakhi, S. Joseph, P. Srivastava, R. Naidu, A. Vinu, Heteroatom functionalized activated porous biocarbons and their excellent performance for CO2 capture at high pressure, J. Mater. Chem. 5 (40) (2017) 21196–21204.
[29] X. Wei, T. Li, Wooden activated carbon production for dioxin removal via a two-step process of carbonization coupled with steam Activation from biomass wastes, ACS Omega 6 (8) (2021) 5607–5618.
[30] A. Ariharan, B. Viswanathan, V. Nandhakumar, Nitrogen-incorporated carbon nanotube derived from polystyrene and polypyrrole as hydrogen storage material, Int. J. Hydrogen Energy 43 (10) (2018) 5077–5088.
[31] P. Selvarajan, M. Fawaz, C. Sathish, M. Li, D. Chu, X. Yu, M.B.H. Breesec, J. Yi, A. Vinu, Activated graphene nanoplatelets decorated with carbon nitrides for efficient electrocatalytic oxygen reduction reaction, Adv. Energy Sustain. Res. https://doi.org/10.1002/aesr.202100104.
[32] M. Ayiania, M. Smith, A.J.R. Hensley, L. Scudiero, J.-S. McEwen, M. Garcia-Perez, Deconvoluting the XPS spectra for nitrogen-doped chars: an analysis from first principles, Carbon 162 (2020) 528–544.
[33] S. Li, Q. Gu, N. Cao, Q. Jiang, C. Xu, C. Jiang, C. Chen, C. Pham-Huu, Y. Liu, Defect enriched N-doped carbon nanoflakes as robust carbocatalysts for H2S selective oxidation, J. Mater. Chem. A 8 (18) (2020) 8892–8902.
[34] K.G. Latham, M.I. Simone, W.M. Dose, J.A. Allen, S.W. Donne, Synchrotron based NEXAFS study on nitrogen doped hydrothermal carbon: insights into surface functionalities and formation mechanisms, Carbon 114 (2017) 566–578.
[35] A. Yanilmaz, A. Tomak, B. Akbali, C. Bacaksiz, E. Ozceri, O. Ari, R.T. Senger, Y. Selamet, H.M. Zareie, Nitrogen doping for facile and effective modification of graphene surfaces, RSC Adv. 7 (45) (2017) 28383–28392, https://doi.org/10.1039/C7RA03046K.
[36] Z. Xing, Z. Ju, Y. Zhao, J. Wan, Y. Zhu, Y. Qiang, Y. Qian, One-pot hydrothermal synthesis of Nitrogen-doped graphene as high-performance anode materials for lithium ion batteries, Sci. Rep. 6 (2016) 26146, 26146.
[37] Z. Song, L. Miao, L. Ruhlmann, Y. Lv, D. Zhu, L. Li, L. Gan, M. Liu, Self-assembled carbon superstructures achieving ultra-stable and fast proton-coupled charge storage kinetics, Adv. Mater. 33 (49) (2021), 2104148.
[38] J. Qu, C. Geng, S. Lv, G. Shao, S. Ma, M. Wu, Nitrogen, oxygen and phosphorus decorated porous carbons derived from shrimp shells for supercapacitors, Electrochim. Acta 176 (2015) 982–988.
[39] S. Zhang, K. Tian, B.-H. Cheng, H. Jiang, Preparation of N-doped supercapacitor materials by integrated salt templating and silicon hard templating by pyrolysis of biomass wastes, ACS Sustain.Chem. Eng. (8) (2017) 6682–6691.
[40] Z. Zhou, L. Miao, H. Duan, Z. Wang, Y. Lv, W. Xiong, D. Zhu, L. Li, M. Liu, L. Gan, Highly active N, O-doped hierarchical porous carbons for high-energy supercapacitors, Chin. Chem. Lett. 31 (5) (2020) 1226–1230.
[41] M. Mansuer, L. Miao, D. Zhu, H. Duan, Y. Lv, L. Li, M. Liu, L. Gan, Facile construction of highly redox active carbons with regular micropores and rod-like morphology towards high-energy supercapacitors, Mater. Chem. Front. 5 (7) (2021) 3061–3072.
[42] W.S. Cha, S.N. Talapaneni, Devaraju M. Kempaiah, S. Joseph, K.S. Lakhi, A.M. Al-Enizi, D.-H. Park, A. Vinu, Excellent supercapacitance performance of 3-D mesoporous carbon with large pores from FDU-12 prepared using a microwave method, RSC Adv. 8 (31) (2018) 17017–17024.
[43] G. Singh, R. Bahadur, A.M. Ruban, J.M. Davidraj, D. Su, A. Vinu, Synthesis of functionalized nanoporous biocarbons with high surface area for CO_2 capture and supercapacitor applications, Green Chem. 23 (15) (2021) 5571–5583.
[44] B. Wadi, A. Golmakani, V. Manovic, S.A. Nabavi, Effect of combined primary and secondary amine loadings on the adsorption mechanism of CO2 and CH4 in biogas, Chem. Eng. J. 420 (2021), 130294.
[45] G. Singh, R. Bahadur, J. Mee Lee, I. Young Kim, A.M. Ruban, J.M. Davidraj, D. Semit, A. Karakoti, A.a.H. Al Muhtaseb, A. Vinu, Nanoporous activated biocarbons with high surface areas from alligator weed and their excellent performance for CO2 capture at both low and high pressures, Chem. Eng. J. 406 (2021), 126787.